Available online at www.sciencedirect.com
ScienceDirect
International Journal of Heat and Mass Transfer 50 (2007) 3913–3924
International Journal of HEAT and MASS TRANSFER
www.elsevier.com/locate/ijhmt

Heat transfer and pressure drop characteristics of laminar air flows moving in a parallel-plate channel with transverse hemi-cylindrical cavities

El Hassan Ridouane *, Antonio Campo

Department of Mechanical Engineering, 201 Votey Hall, The University of Vermont, 33 Colchester Avenue, Burlington, VT 05405, United States

Received 11 January 2006; received in revised form 2 February 2007
Available online 3 April 2007

Abstract

Laminar flows in parallel-plate channels are usually caused by a combination of small channel dimensions and low fluid velocities. As a consequence, the heat transfer coefficients in these channels are extremely low. The present study avoids inward protruding fins attached to the channel walls and instead focuses on the opposite arrangement. That is, molding the walls of parallel-plate channels with arrays of transverse cavities pointing outward. Two configurations were studied, one with symmetrically opposing cavities onto the bottom and upper walls and another with non-symmetric or staggered cavities onto the two parallel walls. A 120-cm-long channel contains two series of 3, 6 and 12 transverse cavities having ratios of cavity depth to cavity print diameter δ/D of 0.125, 0.25, 0.375, and 0.5. Computations are performed for Reynolds numbers based on the hydraulic diameter ranging from 1000 to 2500 for air ($Pr = 0.7$). The finite-volume method is used to perform the computational analysis with embedded second-order-accurate QUICK and SIMPLE schemes. It is found that the cavity/channel assemblies can achieve heat transfer enhancements of about 30% relative to the smooth channel, with pressure loss increases of 19%. In all cases examined, the outcome of the numerical simulation reveals that the heat transfer enhancement overcomes the pressure drop accretion.

Keywords: Parallel-plate channel; Hemi-cylindrical cavities; Heat transfer enhancement; Pressure drop; Vortex formation

1. Introduction

Laminar forced-convection flows in parallel-plate channels have been extensively studied in recent decades. Indeed, this problem poses considerable technological interest in specialized applications subjected to space and/or weight constraints. The most notorious examples are compact heat exchangers (Gnielinski [1] and Sekulic and Shah [2]) and electronic equipment packages (Simons et al. [3], Bar Cohen [4], and Chung et al. [5,6]).

In most parallel-plate channels, it is typical that the flow is laminar due to the combination of small channel dimensions and low fluid velocities. As a consequence, the heat transfer coefficients turns out to be extremely low. To overcome the insufficient heat transfer rates, one idea that has been contemplated is to install transverse fins (or ribs) normal to the main flow. The use of fins brings forward a three-fold objective: (1) to periodically interrupt the hydrodynamic boundary layer, (2) to add surface area and (3) to advect secondary flow and vortex formation. Further, the partial blockage of the channel width increases the flow velocity causing the flow to deflect and impinge against the wall and the subsequent fins. Obviously, the fluid flow versus the heat transfer will be highly sensitive to the geometric fin arrangement used. Representative papers by Berner et al. [7], Webb and Ramadhyani [8], Kelkar and Patankar [9], Lazaridis [10] and Cheng and Huang [11] have dealt with the numerical computation of the heat and fluid flow characteristics of parallel plate channels

* Corresponding author. Tel.: +1 802 656 3304; fax: +1 802 656 1929.
E-mail address: eridouan@cems.uvm.edu (E.H. Ridouane).

0017-9310/$ - see front matter © 2007 Elsevier Ltd. All rights reserved.
doi:10.1016/j.ijheatmasstransfer.2007.02.004

Nomenclature

c_p	air specific heat capacity, J kg^{-1} K^{-1}
D	cavity diameter, m
D_h	hydraulic diameter, (=2H)
E_{HT}	heat transfer performance, Eq. (7)
E_{PD}	pressure drop performance, Eq. (8)
HFP	overall heat/flow performance parameter, Eq. (9)
h	mean heat transfer coefficient, W m^{-2} K^{-1}
H	channel height, m
k	air thermal conductivity, W m^{-1} K^{-1}
L	length of plate plus perimeter of cavities, m
N	number of cavities on each wall
Nu	Nusselt number, ($=hD_h/k$)
p	static pressure, Pa
Pr	Prandtl number, ($=\nu/\alpha$)
q_w	wall heat flux, W m^{-2}
$\overline{q_w}$	mean wall heat flux, W m^{-2}
R	gas constant
Re	Reynolds number, ($=\bar{u}D_h/\nu$)
T	temperature, K
u, v	axial and transverse velocities, m s^{-1}
$\bar{u}$	mean axial velocity, m s^{-1}
$\mathbf{v}$	velocity vector, m s^{-1}
x,y	axial and transverse coordinates, m

Greek symbols

α	air thermal diffusivity, m^2 s^{-1}
δ	cavity depth, m
ν	air kinematic viscosity, m^2 s^{-1}
Δp	pressure drop measured relative to a local static pressure, Pa
ρ	air density, kg m^{-3}

Subscripts

i	condition at the channel inlet
w	condition at the channel wall

having a bundle of normal fins on the side walls. These studies predicted the heat transfer patterns and fluid flow behavior under the assumption of periodic fully developed flow and treated the relative position of the fin as an important variable. It was found that from the standpoint of heat transfer augmentation, the staggered arrangement outperforms the in-line arrangement. From a physical context, this trait is somehow expected because the staggered fins can cause the flow to deflect and impinge upon the opposite walls, whereas the in-line fins make the passing flow detach from the channels, hence reducing the heat transfer performance on the walls. In general, when compared against the smooth parallel-plate channel, all of the above papers consistently showed that reasonable heat transfer enhancement was achievable only at the expense of high pressure drops. As a consequence, this action elevates the power requirement for the pump needed to sustain the desired channel fluid flow. One important conclusion made in [8] was that the invigoration in heat transfer for gases ($Pr \approx 0.7$) is not sufficient to offset the tremendous pressure drop penalty. Nevertheless, from an optimistic framework, the augmentation of heat transfer may be probably justified for high Prandtl number fluids ($Pr \ll 1$) such as water, oils and perhaps fluorocarbons. Pressure drop penalties are often quantified using the overall heat/flow performance (HFP) parameters.

Ghaddar et al. [12] studied idealized two dimensional isothermal cyclic flow in channels with integrated circuits protrusions. Their results show that there exists a critical value of the Reynolds number above which cyclic flow oscillations, which increase fluid transport, are observed. Ghaddar et al. [13] used two dimensional non-isothermal predictions to illustrate the potential for naturally enhancing heat transfer using the unsteadiness observed by Ghaddar et al. [12]. Amon and Mikic [14], and Amon [15] extend the above work, in [12,13], comparing heat transfer enhancement for airflows where oscillations are induced passively and naturally above the Reynolds critic.

The present study avoids the flow perturbation caused by inserting inward protruding fins to the channel walls and instead focuses on the opposite arrangement, that is attaching arrays of transverse cavities pointing outward onto the walls of parallel-plate channels. Related articles to this subject are those of Wirtz et al. [16] and McGarry et al. [17]. At low Reynolds number, the two geometric configurations showed little or no heat transfer enhancement in comparison with the smooth parallel-plate channel. However, with increments in the Reynolds number, longitudinal vortices increased in size resulting in appreciable heat transfer augmentation.

In recent years, designers of a variety of different thermal/fluid systems expressed interest in dimples placed on the surfaces of internal passages because they produce important heat transfer enhancement with relatively smaller pressure drop penalties [18–20]. These authors provided experimental results, measured above a dimpled test surface placed on one wall of a channel for wide ranges of parameters. The controlling parameters considered are Reynolds numbers from 600 to 61,000, ratios of air inlet stagnation temperature to surface temperature from 0.68 to 0.94, and three ratios of channel height to dimple print diameter: 0.25, 0.5, and 1.0. Flow visualizations showed that a vortex pair is periodically shed from the central portion of each dimple. These vortex structures, which augment the local Nusselt numbers near the downstream rims of each dimple, become stronger as the channel height decreases. Later, Won and Ligrani [21] and Park et al. [22] studied numerically the turbulent air flow in channels with

dimples placed on the bottom wall using the k-ε turbulence model under the platform of the commercial code FLUENT. Their results focused on the centrally located vortex pairs near the spanwise edges of individual dimples. The fluid within and near these vortices contains augmented magnitudes of eddy diffusivity for momentum and heat.

The body of the present paper is divided into three sections. The first section describes the physical systems and the mathematical formulation. The computational procedure, the sensitivity of the grid and the code validation are explained in the second section. A discussion of the velocity and temperature fields, via velocity vector plots and temperature plots is reserved for the third section. Also included here are the effects on design quantities such as the pressure drop and the mean heat transfer coefficient. Undoubtedly, this valuable information provides guidance to engineers engaged in the design of ducts for high-performance heat exchange devices.

2. Parallel-plate channel layout

Fig. 1a and b illustrate a two-dimensional parallel-plate channel containing a series of three transverse outward cavities placed onto each wall. Two configurations were studied, one with symmetrically opposing cavities onto the bottom and upper walls (Fig. 1a) and another with non-symmetric or staggered cavities onto the two parallel walls (Fig. 1b). Also, two series with 6 and 12 hemi-cylindrical transverse cavities are studied. For these tests, the total length of the channel is maintained and the distance between the cavities is varied. The spacing between the cavities for 6 and 12 cavity geometries are described in Fig. 1c. Fig. 2 shows the geometric details of the cavities with variable depth δ. The cavity dimensions together with the range of Reynolds numbers tested for each cavity are summarized in Table 1. The dimensions of the channel are 120 cm long and 4 cm height, the cavity print diameter is 2 cm, and the cavity depths are 0.25, 0.5, 0.75, and 1 cm. These combinations give rise to a ratio of channel height to cavity print diameter of 2, and ratios of cavity depth to cavity print diameter δ/D of 0.125, 0.25, 0.375, and 0.5, respectively. It may be noted that the definition of the hydraulic diameter D_h does not account for the localized increased cross-sections caused by the presence of the cavities. This choice permits a direct comparison of the magnitudes of the pressure drop and the heat transfer with those for the smooth channel at the same value of Re.

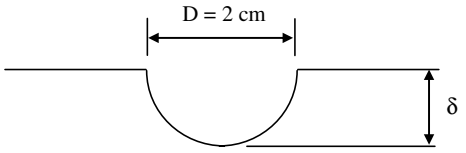

Fig. 2. Geometry of the hemi-cylindrical cavities.

3. Computational procedure

The computational domain is confined to a 120-cm-long channel containing two series of 3, 6 and 12 transverse cavities. The grid is made up of quadrilateral elements aligned with the flow direction to reduce the numerical diffusion

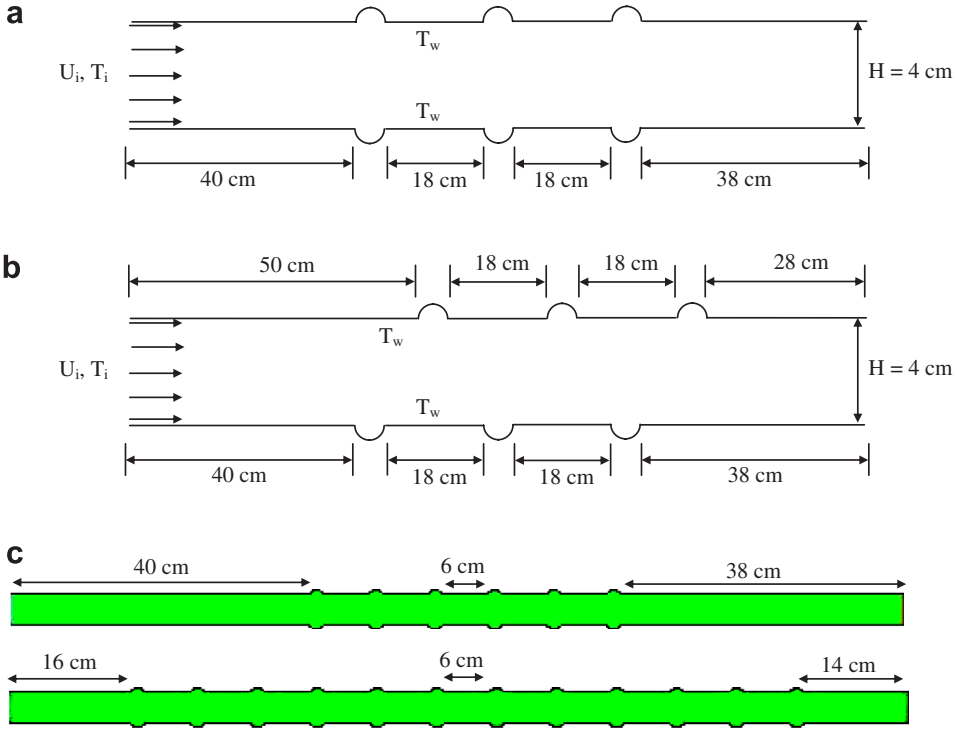

Fig. 1. Schematic of the physical systems: (a) symmetrical arrangement, (b) staggered arrangement, and (c) spacing between 6 and 12 cavities.

Table 1
Dimensions of the cavities for the cases considered

D (cm)	δ/D	N	Re
2	0.125	12	2500
2	0.25	3, 6, 12	1000–2500
2	0.375	12	2500
2	0.5	3, 6, 12	1000–2500

errors and thus improve the quality of the numerical predictions. The regions near the wall and cavity surfaces are meshed with fine grids to resolve the typical high gradients that normally occur there; the nearest grid point next to the surface is within 0.5 mm from the wall and no wall function was used. For a channel with 12 cavities of relative depth $\delta/D = 0.5$, a total of 155,000 finite-volume quadrilateral elements are employed for the entire flow domain to attain grid-independent solutions. For all configuration combinations, the grid-independent mesh sizes are summarized in Table 2. The process of mesh refinement is repeated progressively until insignificant changes in velocity and temperature happen. Statistical analysis of the predicted results is then used to estimate the uncertainty magnitudes. The numerical uncertainty for the two velocity components should be less than 2%, while for the local heat flux, it should be less than 5%. A portion of the computational grid around the second cavity of a 3-cavity channel employed is shown in Fig. 3.

The partial differential equations governing laminar forced convection are reduced to a system of simultaneous algebraic equations by means of the control-volume based finite volume procedure described by Patankar [23]. The discretization of the combined convective and diffusive fluxes across the control surfaces is modeled using the QUICK scheme, which relies on a three-point upstream-weighted quadratic interpolation for cell face values. Since the scheme is based on a quadratic function, its accuracy in terms of Taylor series truncation error is third order [23]. Another notable feature is the fact that the discretized equations involve not only immediate-neighbor nodes but also nodes that are far away. The pressure–velocity coupling is handled with the SIMPLE scheme [23]. Steady-state solutions are obtained utilizing under-relaxation techniques. The full, steady, two-dimensional conservation of mass and momentum equations

Table 2
Computational grids employed for different channels

Number of cavities	Relative cavity depth δ/D	Mesh
0	0	88,000
3	0.25	109,000
	0.5	113,000
6	0.25	122,000
	0.5	128,000
12	0.25	141,000
	0.5	155,000

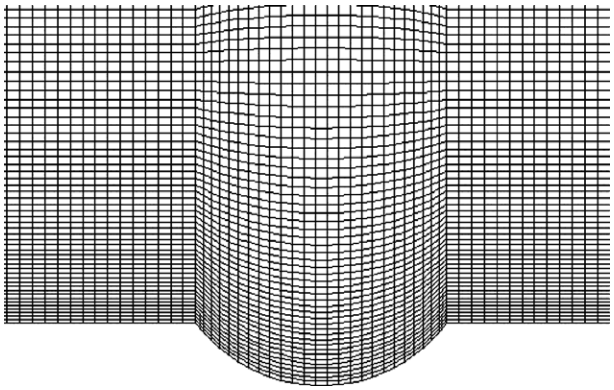

Fig. 3. A portion of the computational grid showing the distribution of elements in a typical channel with $\delta/D = 0.25$.

$$\nabla \cdot (\rho \mathbf{v}) = 0 \tag{1}$$

$$\nabla \cdot (\rho \mathbf{v}\mathbf{v}) = -\nabla p + \nabla \cdot (v \nabla \mathbf{v}) = 0 \tag{2}$$

are solved subject to no-slip boundary conditions at all solid walls, while a uniform velocity U_i was imposed for the inlet boundary condition and a constant pressure of zero gauge for the outlet boundary condition. The companion two-dimensional energy equation is

$$\nabla \cdot (\rho c_P \mathbf{v} T) = \nabla \cdot (k \nabla T) \tag{3}$$

and the ideal gas equation of state is

$$p = \rho R T \tag{4}$$

Constant temperature boundary conditions are employed. In fact, the wall temperature including the cavity surfaces is maintained at $T_w = 320$ K. The cooling fluid is air with a temperature $T_i = 280$ K at the channel inlet. These numbers produce a ratio of inlet temperature to wall temperature of 0.875. The streamwise gradients of all variables such as velocity and temperature were set to zero at the outlet boundary to attain fully developed conditions. In the above equations, the air viscosity and the thermal conductivity vary with the standard power law relation and the specific heat capacity is constant over the expected temperature range.

Computations are performed for Reynolds numbers based on the channel hydraulic diameter ranging from 1000 to 2500 in conjunction with a Prandtl number of 0.7 for air. Local convergence was assessed by point monitors of the velocity and temperature in the vicinity of the first and last cavities on each wall, while global convergence was monitored by the residuals of the mass, momentum and energy conservation equations by setting its variations to less than 10^{-6}.

Once the velocity and temperature fields, $u(x,y)$, $v(x,y)$ and $T(x,y)$ are obtained, the local wall heat flux q_w can be found by specifying Fourier's law at the hot walls. The computation of the mean wall heat flux $\overline{q_w}$ is carried out with the mean value of the function $q_w(x)$ along each wall:

$$\overline{q_w} = \frac{1}{L}\int_{wall} q_w(x)\,dx \tag{5}$$

where q_w is defined based per unit area of the wall. The mean Nusselt number is obtained from the standard definition

$$\overline{Nu} = \frac{\overline{q_w}}{(T_w - T_i)}\left(\frac{D_h}{k}\right) \tag{6}$$

The computer code output was validated first by reproducing the solutions for the velocity and temperature development in a parallel plate channel with smooth surfaces, constant inlet velocity and equal wall temperatures. Based on the given hydraulic diameter, good agreement for the axially changing friction factor and the Nusselt number reported in Shah and London [24] was found. For a fully developed condition the asymptotic values of $fRe/4 = 24$ and $Nu_\infty = 7.54$ were found. A second validation was done against experimental data of air moving over heated rectangular blocks in a two-dimensional channel reported by Herman and Kang [25]. The two-part comparison was based on the mean Nusselt number (Fig. 4a) and the friction factor for the grooved channel (Fig. 4b). Both figures illustrate good parity between the experimental and numerical results varying with the Reynolds number. Among all the *Nu–Re* and *f–Re* data points, the maximum deviation detected is within a tolerable 10% band.

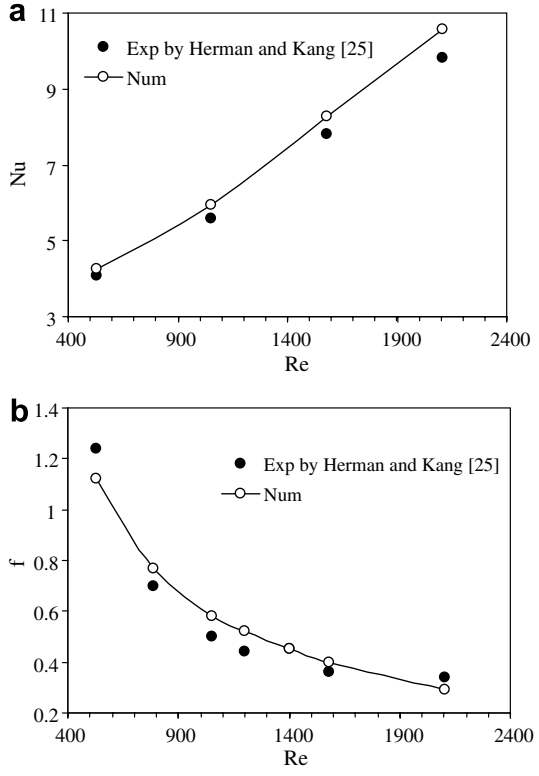

Fig. 4. Comparison between the numerical predictions and the experimental observations over a sequence of heated rectangular blocks in a two-dimensional channel conducted by Herman and Kang [25]: (a) mean Nusselt number and (b) friction factor.

4. Discussion of the numerical results

Flow patterns, heat transfer coefficients, and pressure drop magnitudes have been investigated numerically for flows through straight parallel plate channels with arrays of hemi cylindrical cavities of variable depth $\delta/D = 0.125$, 0.25, 0.375, and 0.5. A series of 3, 6, and 12 cavities are placed on the opposite walls of the channel in both symmetrical and staggered arrangements. The results are compared to those for a standard channel with smooth surfaces. The one-to-one comparison between the symmetrical and staggered arrangements for all channel configurations produced differences in term of heat transfer and pressure drop that are insignificant. Accordingly, the results for the staggered arrangements will be presented for the channel with three cavities only. The fluid flow is assumed to be laminar and Reynolds numbers ranging from 1000 to 2500 have been tested with each type of cavity array and depth.

4.1. Fluid flow

The essential features of the flow induced by the hemicylindrical cavities arranged on the walls of a parallel plates channel can be inferred from Figs. 5 and 6. Fig. 5a and b, on the left, show velocity vectors near the upper surface of the central cavity in a channel with three cavities with $\delta/D = 0.5$ at Reynolds numbers of 1000 and 2500, respectively. The flows for the presented cavity region are representative of flows observed in other cavities throughout the computational domain. Vortical structures can be observed and the fluid is recirculating in the counterclockwise direction (clockwise direction for cavities on the bottom wall). The vector lengths are proportional to local velocity magnitudes. Within the cavity, the velocity magnitudes are much smaller than the average flow velocity. However, the velocity vectors are largest in the central region of the channel and downstream of the cavity. When the Reynolds number is increased to 2500 (Fig. 5b), the qualitative structure of the vortex remains the same as in Fig. 5a despite the augmentation in the velocity vector magnitudes, which are increased in magnitude by a factor of 2. Fig. 5a and b on the right, display the temperature contours for the same Reynolds numbers cited above. The effect of the vortex formation on the shape of the temperature contours can clearly be seen in the regions where the vortices form. Also, it is observable that the isotherms are altered significantly by the presence of the cavity over a distance corresponding to about half of the cavity depth under the cavity horizon.

Fig. 6a–b depict the flow pattern resulting from the vortical structure above the lower wall of the channel just above the central cavity in a channel with three cavities of smaller depth ($\delta/D = 0.25$) for the same Reynolds

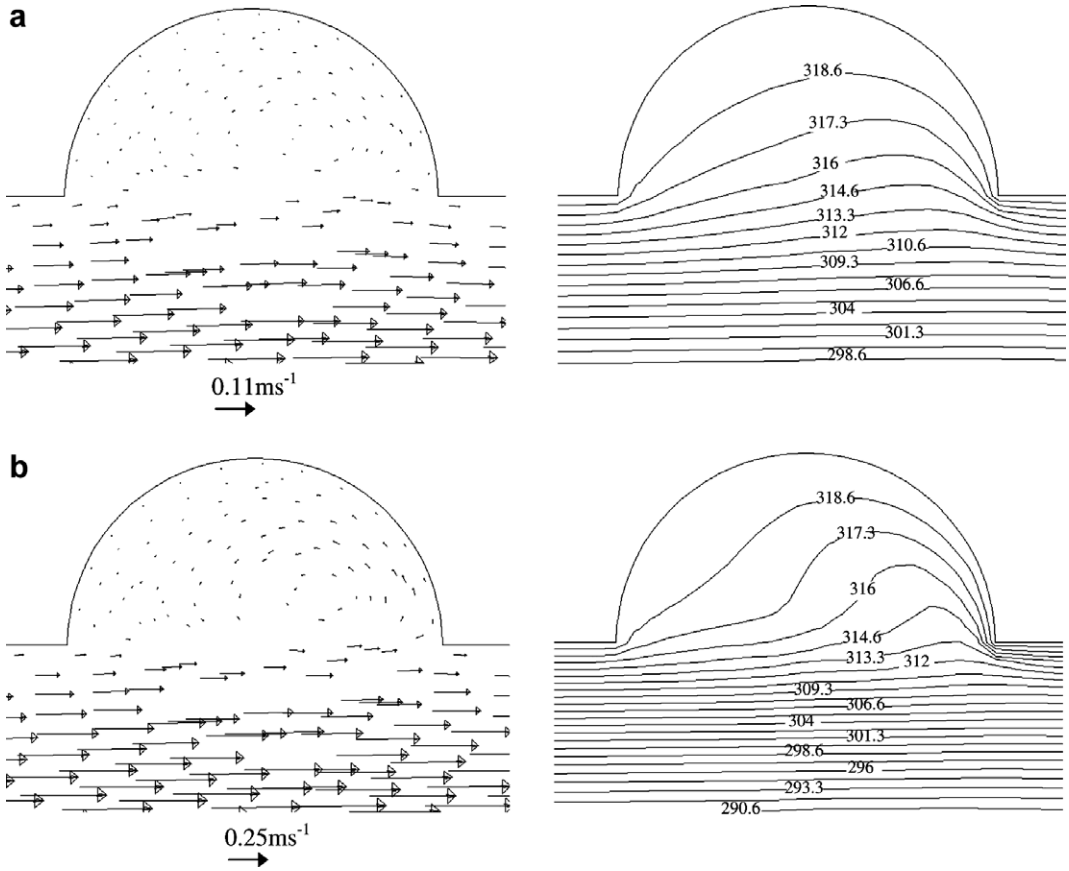

Fig. 5. Velocity vectors and isotherms inside a cavity with full radius depth $\delta/D = 0.5$, $T_i = 280$ K and $T_w = 320$ K: (a) $Re = 1000$ ($\bar{u} = 0.198\ \mathrm{m\,s^{-1}}$) and (b) $Re = 2500$ ($\bar{u} = 0.496\ \mathrm{m\,s^{-1}}$).

numbers cited above. Compared to the cavity with $\delta/D = 0.5$, in addition to a reduced size of the vortex, the magnitudes of the velocity vectors inside the cavity are enlarged resulting in higher vortex strength. In the corresponding isotherm plots on the right, the thermal boundary layer is much thinner at a high Re number near the downstream rim of the cavity as well as on flat surface downstream where high temperature gradients exist. As a result, local heat flux augmentations are specially pronounced in these regions as can be seen in the forthcoming section.

At $Re = 2500$, the vorticity distribution in the flow recirculation zones is depicted in Fig. 7 for $\delta/D = 0.25$ and 0.5. In Fig. 7a, it is seen that two regions of high vorticity are manifested, which are located on the flat surface in the vicinity of the individual cavities. The flat surface upstream presents the highest value of the vorticity with a sharp gradient. However, the flow above the cavity is composed of regions of increasing vorticity (inside the cavity) and decreasing vorticity (outside the cavity). When the cavity depth is reduced to $\delta/D = 0.25$, the vorticity distribution is more complex exhibiting a higher gradient when compared to that of a cavity with $\delta/D = 0.5$. In fact, as the depth of the cavity decreased from $\delta/D = 0.5$ to 0.25, the maximum vorticity increased by a margin of 40%. This pattern is a direct result of the vortex, which is shed from the cavity with higher velocities as confirmed by the velocity vector plot of Fig. 6.

4.2. Heat transfer

Baseline heat transfer results are obtained with a smooth test surface replacing the cavity test surface at the same Reynolds numbers as employed in the channel with cavities. These baseline values are used as a basis of comparison to grooved surface values. Note that the channel height H is measured between the flat portions of the walls. The ratio of channel height to cavity print diameter H/D employed in this study is 0.5. The flow in Figs. 8 and 9 moves from left-to-right.

Regarding the standard channel with smooth surfaces, q_w is highest at the entrance of the channel. As the thermal and velocity boundary layers develop in the streamwise direction, q_w exhibits an exponential decrease that continues to the exit (results not presented). In addition to this standard trend, the q_w-curves related to channels with cavities are more complex and characterized by two peaks at each cavity. Fig. 8 shows the numerically predicted local heat flux distributions along the upper wall of a channel with three cavities on each wall, for $Re = 2500$. The results of both symmetrical and staggered arrangements are pro-

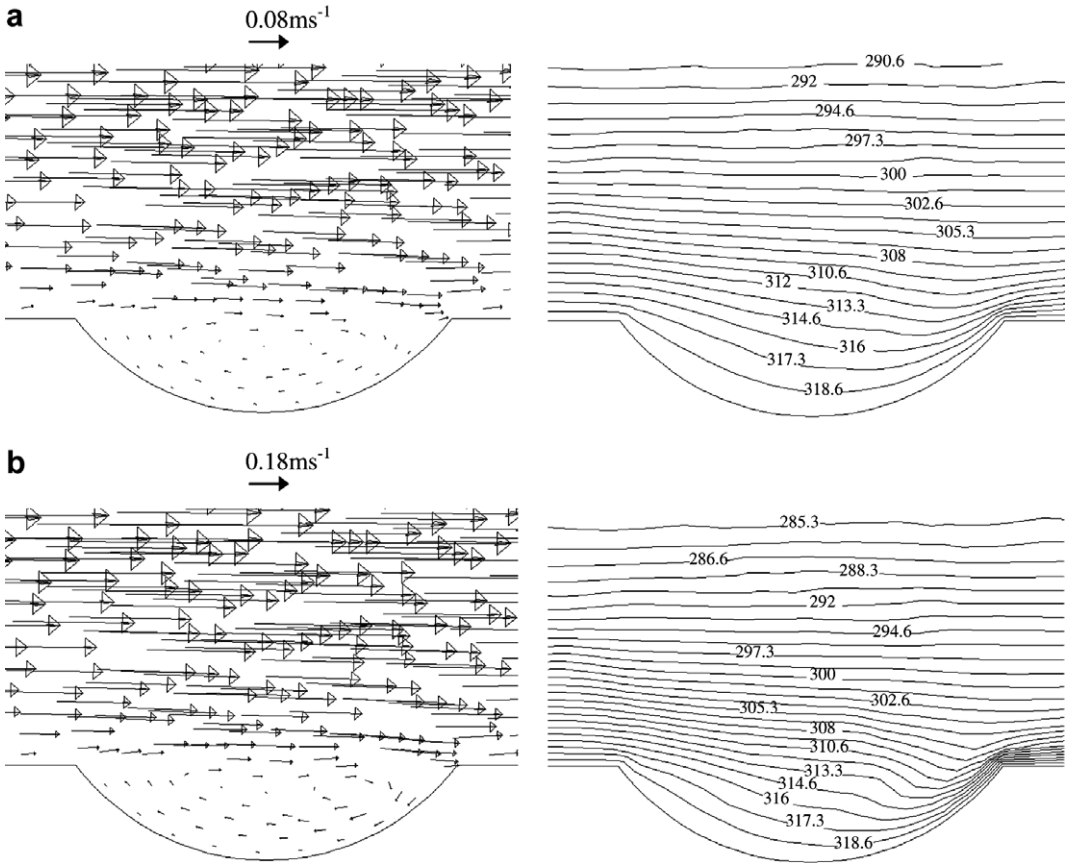

Fig. 6. Velocity vectors and isotherms inside a cavity with half radius depth $\delta/D = 0.25$, $T_i = 280$ K and $T_w = 320$ K: (a) $Re = 1000$ ($\bar{u} = 0.198$ m s^{-1}) and (b) $Re = 2500$ ($\bar{u} = 0.496$ m s^{-1}).

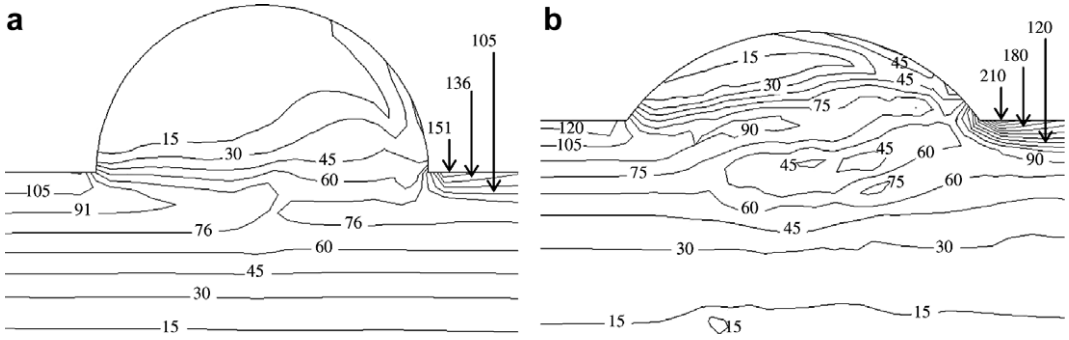

Fig. 7. Plots of the vorticity distribution (s^{-1}) inside a cavity at $Re = 2500$ ($\bar{u} = 0.496$ m s^{-1}), $T_i = 280$ K and $T_w = 320$ K: (a) $\delta/D = 0.5$ and (b) $\delta/D = 0.25$.

vided and compared along the channel. For the sake of differentiating between the different curves, results are given for the symmetrical arrangement around $x = 0.41$ m and the staggered arrangement around $x = 0.51$ m. These x-values correspond to the locations of the center of the first cavity along the flow direction of each arrangement. Notice that regions with the highest local heat fluxes are located just downstream of the cavities. This is due to the prevalent high vorticity at these locations as apparent in Fig. 7. In contrast, regions with lower local heat fluxes are then located within the cavities. These opposing results are confirmed experimentally by Mahmood and Ligrani [18] and Burgess et al. [26] employing a channel with hemispherical dimples. Regarding the q_w-curve related to $\delta/D = 0.5$, the minimum of q_w is about 100 W/m^2 less than the corresponding value of the standard channel. However, the maximum of q_w is about 400 W/m^2 higher. The effect of the cavity depth on the heat flux distribution is obvious and the q_w-curve related to $\delta/D = 0.5$ lies always underneath its counterpart curve related to $\delta/D = 0.25$. This sequence is

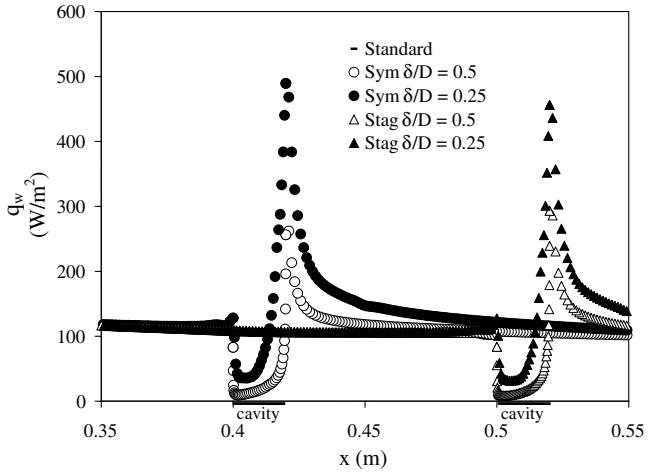

Fig. 8. Local wall heat flux along the upper wall of the channel with three cavities for the two arrangements at $Re = 2500$ ($\bar{u} = 0.496\ \mathrm{m\ s^{-1}}$), $T_i = 280$ K and $T_w = 320$ K.

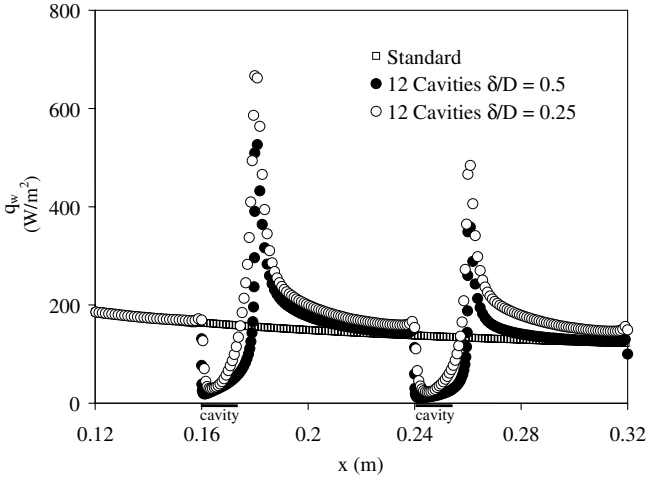

Fig. 9. Local wall heat flux along the upper wall of a channel with 12 cavities. the parameters are $Re = 2500$ ($\bar{u} = 0.496\ \mathrm{m\ s^{-1}}$), $T_i = 280$ K and $T_w = 320$ K.

attributed to the fact that, stronger vortex exists in the cavity with $\delta/D = 0.25$ as confirmed by the vorticity distribution of Fig. 7.

The effect of cavity arrangement (symmetrical or staggered) on q_w is seen to be very limited and the magnitude of the peaks (maximum and minimum) are relatively the same. Thus, the results for channels with 6 and 12 cavities will be limited to the symmetrical arrangement of the cavities only. This minimal effect of the symmetrical and staggered cavity arrangements are due to the use of a $H/D = 2$ channel, which provides minimal interactions between events developing from near the two walls of the channels.

Plotted in Fig. 9 is the local heat flux depending upon the distance along the upper wall of a channel with 12 cavities on each wall when arranged in a symmetrical fashion. These results are presented to demonstrate the influence of both the depth and the location of the cavity, as Reynolds number is held constant at 2500. It is evident that the q_w values increase as δ/D decreases. The increments are especially apparent on the flat surfaces just downstream of each cavity and in the upstream part of the cavity. These changes occur because the vortex existing in the cavity gets stronger as the cavity depth decreases. One further point should be noted about the cavity locations with respect to the channel inlet: the magnitude of the extreme values of the peaks rises as the cavity location gets closer to the inlet. However, the heat transfer enhancement compared to the standard channel stays invariant with respect to the cavity locations because both increments in the extreme values compensate each other.

Fig. 10 illustrates the variation of the mean Nusselt number as a function of *Re* for a channel with three cavities on each wall. The emphasis is given to the heat transfer enhancement of the two arrangements of cavities. The lowermost *Nu* curve representative of the smooth channel presents a monotonic increase with the *Re* number in the whole range of Reynolds considered. The hemi-cylindrical cavities of relative depth $\delta/D = 0.5$ show a very limited enhancement in *Nu* number of about 5% at a low *Re* and 6% at a high *Re*. Both arrangements, symmetrical and staggered, present similar enhancement patterns. When the relative depth is reduced to $\delta/D = 0.25$, the *Nu* curves of the two arrangements climb up slightly and a remarkable gain in the heat transfer enhancement is observed. In numbers, it goes up to about 9% at a low *Re* and to about 13% at a high *Re*. These results are taken in reference to the smooth channel. More details about how this gain varies with *Re*, the relative cavity depth as well as type of arrangement are listed in Table 3.

Having established the results within a channel with three cavities and knowing that both arrangements induce similar enhancement levels, the focus shifts to the effect of the number of cavities on the overall heat transfer. Two series of channels were considered, one with 6 cavities on

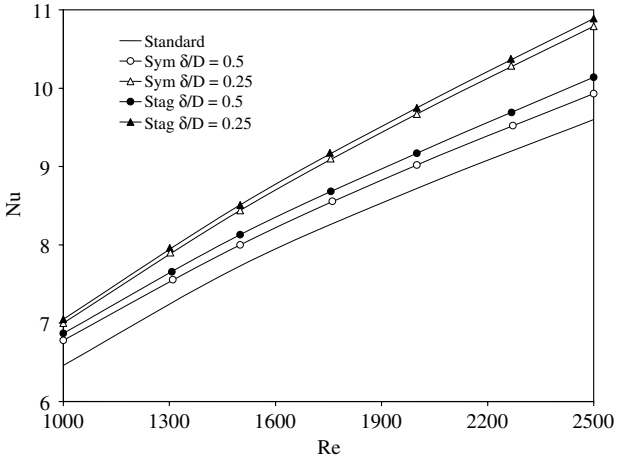

Fig. 10. Variations of the mean Nusselt number with the Reynolds number for the two arrangements and different cavity depths in a channel with three cavities: $T_i = 280$ K and $T_w = 320$ K.

Table 3
Heat transfer enhancement delivered by a channel with three cavities relative to the standard smooth channel (%)

Re	2500	2000	1500	1000
Sym $\delta/D = 0.5$	3.44	3.44	3.50	4.95
Sym $\delta/D = 0.25$	12.40	10.90	9.18	8.36
Stag $\delta/D = 0.5$	5.63	5.16	5.17	6.35
Stag $\delta/D = 0.25$	13.43	11.82	10.10	9.13

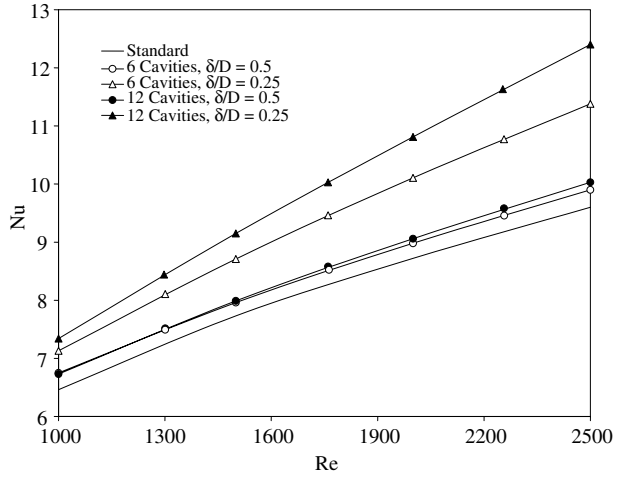

Fig. 11. Variations of the mean Nusselt number with the Reynolds number in a channel with 6 and 12 cavities for different cavity depths: $T_i = 280$ K and $T_w = 320$ K.

each wall and the other with 12 cavities and the outcomes are illustrated in Fig. 11. Here again, the *Nu* curve of the standard channel is the lowest and considered as baseline for comparison purposes. The mean Nusselt number of the wall containing cavities of relative depth $\delta/D = 0.5$ is not affected by the number of cavities. Series of 6 and 12 cavities provide equal heat transfer performance, which is similar to the ones reflected in Fig. 10 with three cavities only. However, as the relative depth decreases to $\delta/D = 0.25$, the gain in heat transfer grows as the number of cavities is elevated. Enhancement of about 18% for the channel with 6 cavities is obtained at a high *Re* number of 2500. This value climbs up to about 30% for the channel with 12 cavities. Table 4 summarizes the heat transfer enhancement as a function of the number of cavities and relative cavity depth.

Table 4
Heat transfer enhancement delivered by channels with 6 and 12 cavities relative to the standard smooth channel (%)

Number of cavities	*Re* =	2500	2000	1500	1000
6	$\delta/D = 0.5$	3.13	3.10	2.98	4.49
	$\delta/D = 0.25$	18.54	15.90	12.68	10.37
12	$\delta/D = 0.5$	4.50	3.90	3.37	4.18
	$\delta/D = 0.25$	30.43	23.97	18.37	13.62

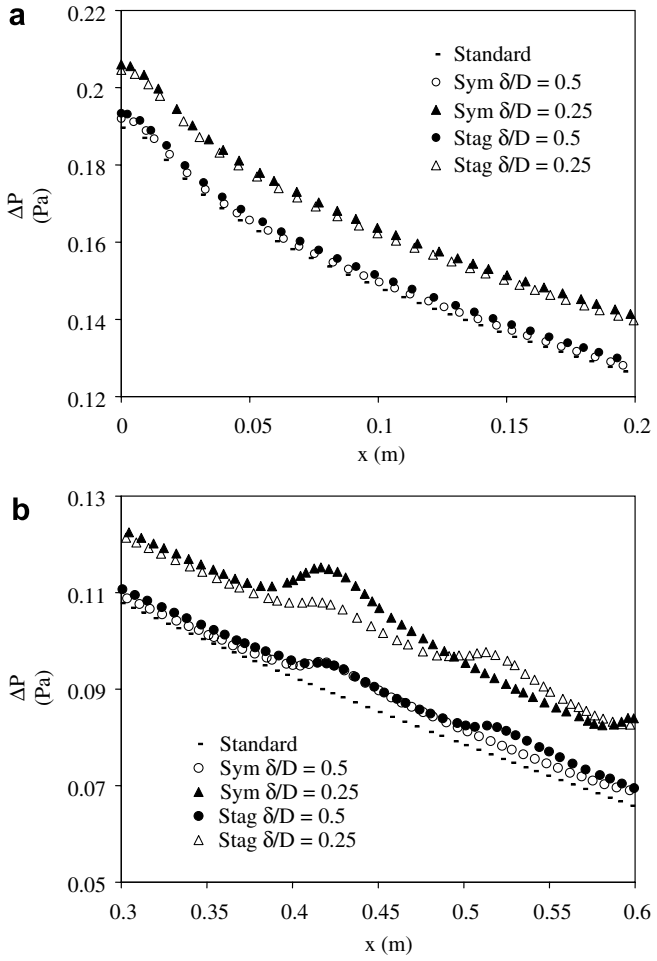

Fig. 12. Local static pressure along the plane of symmetry from the inlet to the exit of a channel with three cavities for the two arrangements and different cavity depths. The parameters are $Re = 2500$ ($\bar{u} = 0.496$ m s^{-1}), $T_i = 280$ K and $T_w = 320$ K.

4.3. Pressure drop

As for the heat transfer enhancement, the increment in the pressure drop is the result of changing the surface of the wall by adding cavities. The local static pressure variation along the channel mid plane is compared for the highest *Re* tested in this study. Shown in Fig. 12 are the three cavity-channel pressure distributions of both arrangements at the inlet (Fig. 12a) and in the region of the first cavity for each arrangement (Fig. 12b). Immediately apparent is the increase in the inlet head required by all cavities cases in order to achieve the same flow rate as that of the smooth channel. In the cavity region, a remarkable increase is represented by a peak of static pressure around each cavity. The cavities with $\delta/D = 0.5$ have a very limited effect on the pressure distribution compared to the standard case; it is higher at the cavity location and also downstream of each cavity. The cavities with $\delta/D = 0.25$ provide a pronounced effect on the pressure drop and require higher inlet pressure.

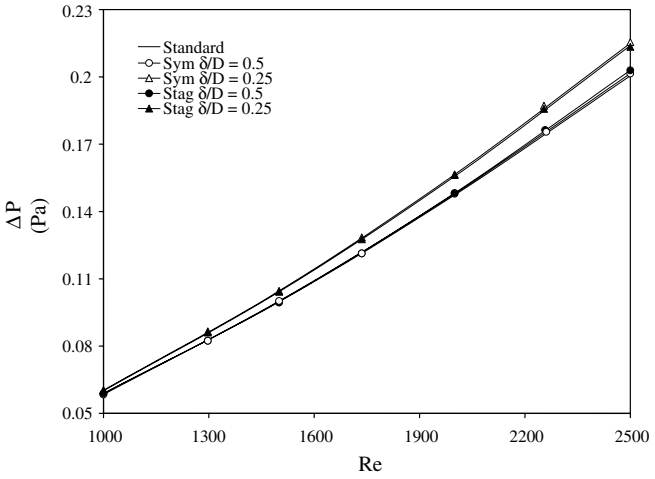

Fig. 13. Variations of the pressure drop with the Reynolds number for the two channel arrangements with three cavities and two cavity depths: $T_i = 280$ K and $T_w = 320$ K.

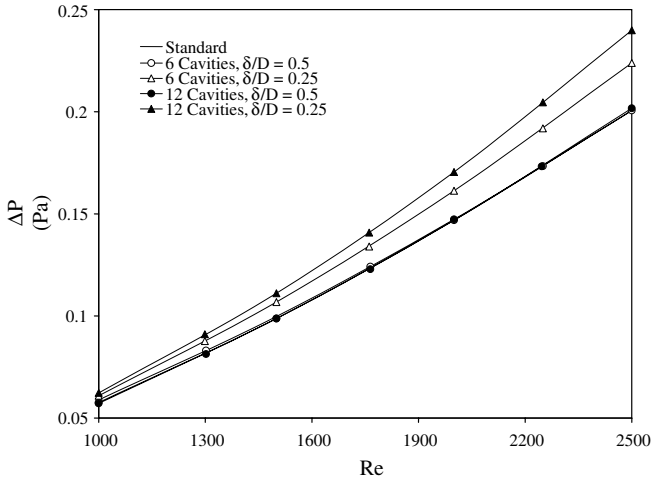

Fig. 14. Variations of the pressure drop with the Reynolds number for a channel with 6 and 12 cavities for different cavity depths: $T_i = 280$ K and $T_w = 320$ K.

Fig. 13 illustrates the variations of the pressure drop with Re for the channel with three cavities on each wall. When compared to the smooth channel, increments in the pressure drop ΔP of less than 0.8% are observed within channels with $\delta/D = 0.5$ for $Re \leqslant 2200$. However, above this value an increment of about 1.2% was required in the inlet pressure. Moreover, the ΔP curves representative of channels with $\delta/D = 0.25$ climb up and deviate from the base curve inherent to the smooth channel. The deviation of these curves increases with the Reynolds number. These geometries require about 2% at a low Re of 1000 and 6% higher inlet pressure at a high Re of 2500. As it happened with the heat transfer in Fig. 10, the type of arrangement does not affect ΔP. Table 5 lists the percent increments of ΔP for the two configurations with three cavities. These values are reported with reference to the smooth channel and the negative values indicate inlet pressures requirements that are less than the corresponding values required by the smooth channel.

The effects of having more cavities on opposite walls can be discerned by comparing the results for 6 and 12 cavities (Fig. 14). Here again, the pressure drop in channels with deeper cavities ($\delta/D = 0.5$) presents a behavior similar to the smooth channel. However, as the depth is reduced to $\delta/D = 0.25$, the influence of the number of cavities is more pronounced. ΔP rises as the number of cavities increases. The increment in ΔP is also favored by increasing Re. The increase in the static pressure at the channel inlet required to achieve the same flow rate as that of the smooth channel is depicted in Table 6. At higher Reynolds number, increments of about 11% are observed in a 6 cavity channel. This value goes up to 19% when the number is doubled to 12 cavities.

Table 5
Incremental in pressure drop of the channel with three cavities relative to the standard smooth channel (%)

$Re =$	2500	2000	1500	1000
Sym $\delta/D = 0.5$	0.49	0.40	0.40	−0.84
Sym $\delta/D = 0.25$	7.21	6.24	4.91	2.37
Stag $\delta/D = 0.5$	1.19	0.61	0.20	0.00
Stag $\delta/D = 0.25$	6.68	5.70	4.51	2.03

Table 6
Increment in pressure drop of the channels with 6 and 12 cavities relative to the standard smooth channel (%)

Number of cavities	$Re =$	2500	2000	1500	1000
6	$\delta/D = 0.5$	0.00	−0.27	−1.00	−2.20
	$\delta/D = 0.25$	11.00	9.50	6.32	3.39
12	$\delta/D = 0.5$	0.59	−0.30	−1.00	−2.88
	$\delta/D = 0.25$	19.20	15.25	10.33	5.70

Overall, the collection of results demonstrates that the presence of cavities can achieve heat transfer enhancements of about 30% relative to the smooth surface case, with pressure losses of about 19%. Moreover, even when the heat transfer intensification is moderate, the pressure loss increment is always smaller.

4.4. Optimal groove depth

From the collection of heat transfer results presented in Section 4.2, it is clear that the enhancement over a flat plate channel increases as the cavity depth goes to zero. However, if the depth is exactly zero, this condition will match the flat plate channel with the minimum heat transfer. Consequently, there must be some optimum cavity depth that maximizes the heat transfer. Multiple tests were conducted in a channel with 12 cavities at $Re = 2500$ for various cavity depths δ/D of 0.125, 0.25, 0.375, and 0.5. The outcome of these tests in terms of the mean heat flux $\overline{q_w}$ and its accompanying pressure drop ΔP are presented in Fig. 15 as a function of δ/D. The path of these curves demonstrates that there is an optimum cavity depth $\delta/D = 0.25$ corre-

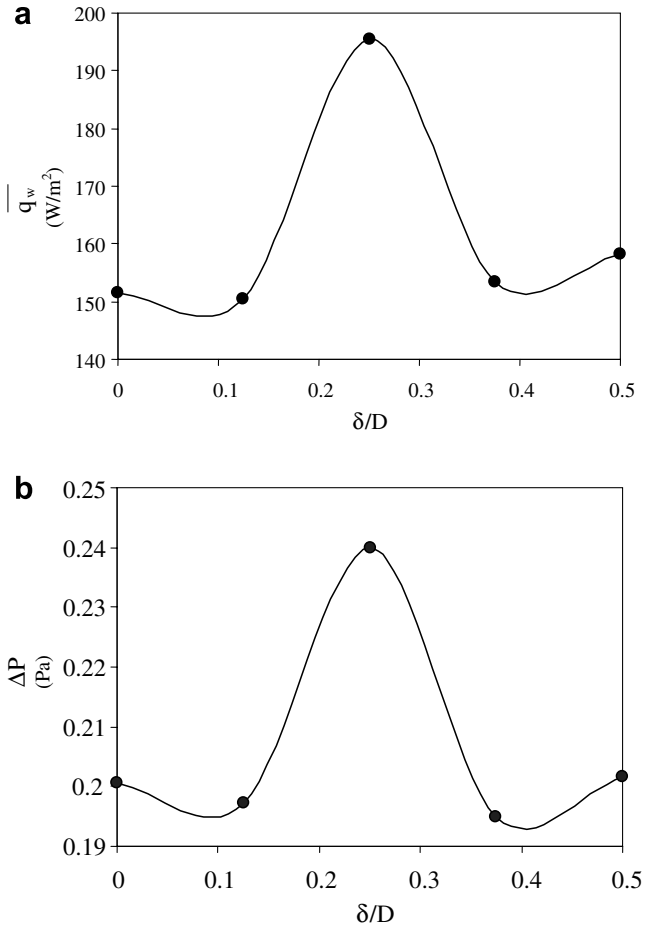

Fig. 15. Optimal cavity depth that maximizes the heat transfer through the channel.

sponding to the maximum of $\overline{q_w}$. The ΔP curve follows the footsteps of the $\overline{q_w}$ curve, but the percent increments of ΔP are always less than those for $\overline{q_w}$.

4.5. Heat transfer and pressure drop performances

Webb [27] proposed a pair of representative ratios for the quantification of the heat transfer efficiency and the pressure drop efficiency, which are useful for engineering analysis and design. The heat transfer performance E_{HT} for a channel with cavities relative to a smooth channel is defined as follows:

$$E_{HT} = \frac{h_{CC}}{h_{SC}} \tag{7}$$

where h_{CC} stands for the heat transfer coefficient of a channel with cavities, while h_{SC} stands for the heat transfer coefficient of a smooth channel. In the quest for heat transfer enhancement, the goal is to procure values of E_{HT} greater than one.

Likewise, the pressure drop performance E_{PD} in a channel with cavities relative to a smooth channel is defined as:

Table 7
Heat/flow quantities for channels with 6 and 12 cavities for $Re = 2500$ and a relative depth $\delta/D = 0.25$

Number of cavities	E_{HT}	E_{PD}	HFP
6	1.19	1.11	1.07
12	1.31	1.19	1.1

$$E_{PD} = \frac{\Delta P_{CC}}{\Delta P_{SC}} \tag{8}$$

Here, ΔP_{CC} denotes the pressure drop in a channel with cavities and ΔP_{SC} denotes the pressure drop in a smooth channel. In the pursuit of pressure drop reductions, the aim is to secure values of E_{PD} equal or slightly less than one.

In view of the foregoing, the overall attributes of the laminar air flow with heat transfer may be combined in an orderly fashion by encapsulating E_{HT} and E_{PD} into a single figure-of-merit parameter, the overall heat/flow performance (HFP) given by:

$$\mathrm{HFP} = \frac{E_{HT}}{E_{PD}} \tag{9}$$

Actually, a channel with cavities is regarded as a good channel for heat transfer augmentation with moderate pressure drop accretion if the channel has HFP values that exceed one. In this regard, Table 7 lists the trio of quantities E_{HT}, E_{PD} and HFP associated with a typical case owing $Re = 2500$ in reference to Figs. 11 and 14. Herein, it is observable that the HFP values exceed one regardless of the relative cavity depth.

5. Conclusions

Laminar air flows in parallel-plates channels with cavities placed on both walls are numerically analyzed and compared using finite volume method. The velocity and temperature fields are given to provide information on the effects of the number of cavities and their depth on the local flow structure, and on local and mean surface heat flux distributions, as well as on the pressure drop between the inlet and the exit of the channel. Different series of 3, 6, and 12 symmetrical and staggered rows of hemi-cylindrical cavities were placed on each wall of the channel. The Reynolds number based on the hydraulic diameter ranged from 1000 to 2500. The ratio of channel height to cavity (groove) print diameter, H/D is 0.5, and the ratios of cavity depth to cavity print diameter δ/D are 0.125, 0.25, 0.375 and 0.5.

Steady-state results show that the streamwise vorticity distributions associated with the flow recirculation zone exist in each cavity and the vortices get stronger as the relative cavity depth approaches $\delta/D = 0.25$. Regardless of the relative cavity depth and the controlling Reynolds number, each cavity contains only one single vortex that rotates clockwise within cavities placed on the bottom wall and in the opposite direction within cavities placed on the upper wall. This phenomena lead to local wall heat flux

augmentations which are especially pronounced near the downstream rim of each cavity. Local wall heat flux augmentations also develop as the vertical fluid advects colder fluid from the central part of the channel to regions near the heated cavity surface. The phenomenon intensifies as the relative cavity depth approaches its optimum $\delta/D = 0.25$, which maximizes the heat transfer throughout the channel.

The mean Nusselt number indicative of total heat transfer and the pressure drop results show that both arrangements (symmetrical or staggered) provide similar results. In addition, when $\delta/D = 0.5$, the number of cavities placed on each wall has no bearing on the mean Nusselt number and pressure drop. However, these global quantities increase as the number of cavities goes from 3 to 12 when the cavities have smaller depth $\delta/D = 0.25$. Overall, the proposed modified channel can achieve heat transfer enhancement of about 30% relative to the smooth surface, with pressure loss increments of 19%. Moreover, even when the heat transfer gain is small the pressure loss increment is always smaller.

References

[1] V. Gnielinski, Forced convection in ducts, in: G.F. Hewitt (Ed.), Handbook of Heat Exchanger Design, Begell House, New York, 1998, Chapter 4.

[2] D.P. Sekulic, R.K. Shah, Fundamentals of Heat Exchanger Design, Wiley, New York, 2002.

[3] R.E. Simons, V.W. Antonnetti, W. Nakayawa, S. Oktay, Heat transfer in electronic packages, in: R.R. Tummala (Ed.), Handbook of Microelectronics Packaging, second ed., Chapman and Hall, New York, 1997, pp. 1.315–1.403.

[4] A. Bar-Cohen, A.A. Watwe, R.S. Prasher, Heat transfer in electronic equipment, in: A. Bejan, A.D. Kraus (Eds.), Handbook of Heat Transfer, Wiley, New York, 2003, Chapter 13.

[5] Y.M. Chung, P.G. Tucker, K.H. Luo, Large-eddy simulation of complex internal flows, in: B.J. Geurts, R. Friedrich, O. Metais (Eds.), Direct and Large-Eddy Simulations IV, Kluwer Academic Publishers, The Netherlands, 2001.

[6] Y.M. Chung, K.H. Luo, N.D. Sandham, Numerical study of momentum and heat transfer in unsteady impinging jets, Int. J. Heat Fluid Flow 23 (2002) 592–600.

[7] C. Berner, F. Durst, D.M. McEligot, Flow around baffles, J. Heat Transfer 106 (1984) 743–749.

[8] B.W. Webb, S. Ramadhyani, Conjugate heat transfer in a channel with staggered ribs, Int. J. Heat Mass Transfer 28 (1985) 1679–1687.

[9] K.M. Kelkar, S.V. Patankar, Numerical prediction of flow and heat transfer in a parallel plate channel with staggered fins, J. Heat Transfer 109 (1987) 25–30.

[10] A. Lazardis, Heat transfer correlation for flow in a parallel plate channel with staggered fins, J. Heat Transfer 110 (1988) 801–802.

[11] C.H. Cheng, W.H. Huang, Laminar forced convection flows in horizontal channels with transverse fins placed in the entrance region, Num. Heat Transfer, Part A 16 (1989) 77–100.

[12] N.K. Ghaddar, K.Z. Karczak, B.B. Mikic, A.T. Patera, Numerical investigation of incompressible flow in grooved channels, Part 1. Stability and self-sustained oscillations, J. Fluid Mech. 163 (1986) 99–127.

[13] N.K. Ghaddar, M. Megan, B.B. Mikic, A.T. Patera, Numerical investigation of incompressible flow in grooved channels, Part 2. Resonance and oscillatory heat-transfer enhancement, J. Fluid Mech. 168 (1986) 541–567.

[14] C.H. Amon, B.B. Mikic, Numerical prediction of convective heat transfer in self-sustained oscillatory flows, J. Thermophys. Heat Transfer 4 (1990) 239–246.

[15] C.H. Amon, Heat transfer enhancement by flow destabilization in electronic chip configurations, J. Electron. Packag. 144 (1992) 35–40.

[16] R.A. Wirtz, F. Huang, M. Greiner, Correlation of fully developed heat transfer and pressure drop in a symmetrically grooved channel, J. Heat Transfer 121 (1999) 236–238.

[17] M. McGarry, A. Campo, D.L. Hitt, Numerical simulations of heat and fluid flow in grooved channel with curved vanes, Num. Heat Transfer, Part A 46 (2004) 41–54.

[18] P.M. Mahmood, P.M. Ligrani, Heat transfer in a dimpled channel: combined influences of aspect ratio, temperature ratio, Reynolds number, and flow structure, Int. J. Heat Mass Transfer 45 (2002) 2011–2020.

[19] P.M. Ligrani, J.L. Harrison, G.I. Mahmood, M.L. Hill, Flow structure due to dimple depressions on a channel surface, Phys. Fluids 13 (2001) 3442–3451.

[20] G.I. Mahmood, M.L. Hill, D.L. Nilson, P.M. Ligrani, H.K. Moon, B. Glezer, Local heat transfer and flow structure on and above a dimpled surface in a channel, ASME J. Turbomach. 123 (2001) 115–123.

[21] S.Y. Won, P.M. Ligrani, Numerical predictions of flow structure and local Nusselt number ratios along and above dimpled surfaces with different dimple depths in a channel, Num. Heat Transfer 46 (2004) 549–570.

[22] J. Park, P.R. Desam, P.M. Ligrani, Numerical predictions of flow structure above a dimpled surface in a channel, Num. Heat Transfer 45 (2004) 1–20.

[23] S.V. Patankar, Numerical Heat Transfer and Fluid Flow, Hemisphere, Washington, DC, 1980.

[24] R.K. Shah, A. A London, Laminar Flow and Heat Transfer in Ducts, Academic, New York, 1978.

[25] C. Herman, E. Kang, Experimental visualization of temperature fields and study of heat transfer enhancement in oscillatory flow in a grooved channel, Heat Mass Transfer 37 (2001) 87–99.

[26] N.K. Burgess, M.M. Oliveira, P.M. Ligrani, Nusselt number behavior on deep dimpled surfaces within a channel, J. Heat Transfer 125 (2003) 11–18.

[27] R.L. Webb, Principles of Enhanced Heat Transfer, Taylor & Francis, New York, 2005.